Title

Reinterpretation of the vibrational spectroscopy of the medicinal bioinorganic synthon c,c,t-[Pt(NH3)2Cl2(OH)2]

Permalink

https://escholarship.org/uc/item/2792r849

Journal

JBIC Journal of Biological Inorganic Chemistry, 19(4-5)

ISSN

0949-8257

Authors

Johnstone, Timothy C
Lippard, Stephen J

Publication Date

2014-06-01

DOI

10.1007/s00775-014-1109-6

Peer reviewed

Reinterpretation of the Vibrational Spectroscopy of the Medicinal Bioinorganic Synthon *c,c,t*-[Pt(NH₃)₂Cl₂(OH)₂]†

Timothy C. Johnstone and **Stephen J. Lippard**
Department of Chemistry, Massachusetts Institute of Technology, 77 Massachusetts Avenue, Cambridge, MA 02139, USA

Stephen J. Lippard: lippard@mit.edu

Abstract

The Pt(IV) complex c,c,t-[Pt(NH$_3$)$_2$Cl$_2$(OH)$_2$] is an important intermediate in the synthesis of Pt(IV) anticancer prodrugs and has been investigated as an anticancer agent in its own right. An analysis of the vibrational spectroscopy of this molecule was previously reported [Faggiani *et al*., **1982**, *Can. J. Chem. 60*, 529] in which crystallographic determination of the structure of the complex permitted a site group approach. The space group, however, was incorrectly assigned. In the present study we have redetermined at high resolution crystal structures of c,c,t-[Pt(NH$_3$)$_2$Cl$_2$(OH)$_2$] and c,c,t-[Pt(NH$_3$)$_2$Cl$_2$(OH)$_2$]·H$_2$O$_2$, which enable discussion of the effect of hydrogen bonding on the N–H and O–H vibrational bands. The correct crystallographic site symmetry of the platinum complex in the c,c,t-[Pt(NH$_3$)$_2$Cl$_2$(OH)$_2$] structure is employed to conduct a new vibrational analysis using both group theoretical and modern DFT methods. This analysis reveals the nature and symmetry of the "missing band" described in the original publication and suggests a possible explanation for its disappearance.

Keywords

oxoplatin; anticancer; vibrational spectroscopy; crystallography

Introduction

The complex c,c,t-[Pt(NH$_3$)$_2$Cl$_2$(OH)$_2$] is a valuable synthetic intermediate in the preparation of Pt(IV) anticancer prodrugs [1]. The nucleophilicity of the coordinated hydroxide ligands permits attack of their oxygen atoms on electrophilic centers in molecules such as acid chlorides, acid anhydrides, pyrocarbonates, and isocyanates [2]. In one design paradigm, the nucleophilic attack opens a cyclic anhydride, such as succinic anhydride, to generate a pendant carboxylate, which can undergo subsequent derivatization [3, 4].

c,c,t-[Pt(NH$_3$)$_2$Cl$_2$(OH)$_2$] has also been studied as an anticancer agent in its own right and in this context is sometimes referred to as oxoplatin [5]. As with the majority of other Pt(IV) compounds that are tested for anticancer activity, it is presumed that the octahedral Pt(IV)

center undergoes reduction with loss of two ligands to produce an active square-planar Pt(II) species [6]. The strongly basic hydroxide ligands stabilize the Pt(IV) oxidation state as evidenced by the very negative cathodic peak potential of less than -800 mV vs. $Ag^+/AgCl$ observed during cyclic voltammetry experiments [7]. Although electrochemical measurements of the irreversible two-electron reduction of Pt(IV) to Pt(II) do not provide a direct measure of the facility of reduction in a biological milieu [8], when c,c,t-$[Pt(NH_3)_2Cl_2(OH)_2]$ is administered intravenously to mice, 50% of the platinum excreted over the course of 5 h is the unchanged Pt(IV) complex [9]. In contrast, c,c,t-$[Pt(NH_3)(c$-$NH_2C_6H_{11})Cl_2(O_2CCH_3)_2]$ has a half-life of only 6.3 min in whole human blood [10].

In this issue dedicated to the memory of Ivano Bertini, we present a reinvestigation of the vibrational spectroscopy of c,c,t-$[Pt(NH_3)_2Cl_2(OH)_2]$. Although Bertini was perhaps best known for his NMR spectroscopic work on paramagnetic metalloproteins [11], his early studies focused on exploring fundamental properties of traditional small molecule coordination complexes. His first published paper [12], and a series that closely followed [13–15], describe the vibrational spectroscopy of transition metal complexes. Vibrational spectroscopy has long served inorganic chemists as a valuable source of information about structure and bonding [16]. Bioinorganic chemists in particular have benefitted not only from advanced techniques such as resonance Raman and nuclear resonance vibrational spectroscopy (NRVS) but also from simple yet powerful IR and Raman spectroscopic experiments [17].

A detailed analysis of the vibrational spectroscopy of c,c,t-$[Pt(NH_3)_2Cl_2(OH)_2]$ was first reported by Rosenberg and coworkers [18]. The report also described the determination of the crystal structure of the compound by X-ray diffraction. The vibrational analysis was accordingly performed using the site symmetry of the complex. Shortly thereafter, the structure was redetermined at higher resolution by Sadler *et al.* [19] and the space group selection in this latter paper was corrected by Marsh [20]. The true space group is not $P4_2/n$, as initially reported in both previous papers, but rather $P4_2/nmc$ owing to the presence of an overlooked c-glide plane. Marsh wrote his commentary in reference to the paper by Sadler and coworkers and only mentions in passing the earlier structural determination by Rosenberg *et al*. Of note is the lack of commentary on the influence that the change in space group may have on the vibrational analysis.

We were particularly drawn to a "missing band" initially reported in the analysis of the vibrational spectrum of the deuterated analog of c,c,t-$[Pt(NH_3)_2Cl_2(OH)_2]$. Given that this study was conducted using the incorrect site symmetry, it seemed possible that the change in space group might provide insight into the nature of this band and its disappearance.

We describe here a reinterpretation of the vibrational spectroscopy of c,c,t-$[Pt(NH_3)_2Cl_2(OH)_2]$ in light of the proper space group, which alters the site symmetry of the molecules in the crystal. IR spectroscopy is combined with single crystal and powder X-ray diffraction methods, as well as group theoretical and density functional theoretical (DFT) calculations, to shed light on this problem. We think that Ivano, given his early and lasting interests in spectroscopy, might have been pleased with the outcome.

Experimental Section

Materials

The compounds c,c,t-[Pt(NH$_3$)$_2$Cl$_2$(OH)$_2$] and c,c,t-[Pt(NH$_3$)$_2$Cl$_2$(OH)$_2$]·H$_2$O$_2$ were prepared as previously described [21, 22]. Briefly, cisplatin was heated to 75 °C in the presence of excess aqueous hydrogen peroxide for 3 h. The solvent volume was reduced in vacuo and the resulting suspension cooled overnight to 4 °C. The solid was collected by filtration and the yellow filtrate set aside. The solid was washed with water, stirred in a minimal amount of boiling water for 10 min, and allowed to cool to room temperature. The yellow microcrystalline solid, c,c,t-[Pt(NH$_3$)$_2$Cl$_2$(OH)$_2$], was collected by filtration, washed with water, ethanol, and diethyl ether, and then dried in vacuo. The yellow filtrate initially set aside from the primary reaction mixture was allowed to stand at 4 °C for 1 week. Large, very pale yellow plates of c,c,t-[Pt(NH$_3$)$_2$Cl$_2$(OH)$_2$]·H$_2$O$_2$ formed. The identities of both crystalline forms were confirmed by single crystal X-ray diffraction. The deuterated analog c,c,t-[Pt(ND$_3$)$_2$Cl$_2$(OD)$_2$] was prepared by stirring c,c,t-[Pt(NH$_3$)$_2$Cl$_2$(OH)$_2$] in D$_2$O at 70 °C for 24 h and isolated as described above.

Physical Measurements

The lack of H$_2$O$_2$ solvate in samples of c,c,t-[Pt(NH$_3$)$_2$Cl$_2$(OH)$_2$] was confirmed by X-ray powder diffraction (*vide infra*) prior to the acquisition of IR spectra. FTIR spectra were collected at a nominal resolution of 1.0 cm^{-1} on a ThermoNicolet Avatar 360 spectrophotometer using the *OMNIC* software. Samples were prepared as KBr pellets and band values are reported in wavenumbers (cm^{-1}). The Raman values discussed below are those previously reported [18].

X-ray Crystallography

Single crystals of c,c,t-[Pt(NH$_3$)$_2$Cl$_2$(OH)$_2$] were obtained directly from the recrystallization flask. Single crystals of c,c,t-[Pt(NH$_3$)$_2$Cl$_2$(OH)$_2$]·H$_2$O$_2$ were obtained from the cooled reaction filtrate as described above. Samples suitable for X-ray diffraction analysis were selected under crossed-polarizers, mounted on a nylon cryoloop in Paratone oil, and cooled to 100 K under a stream of nitrogen. A Bruker APEX CCD X-ray diffractometer controlled by the *APEX2* software [23] was used to collect data from the crystals using graphite-monochromated Mo Kα radiation (λ = 0.71073 Å). After integration with *SAINT* [24], absorption, Lorentz, and polarization corrections were applied by using *SADABS* [25]. Space groups were determined by analyzing the metric symmetry and systematic absences of the diffraction pattern with *XPREP* [26]. Using the *SHELXTL-97* software package [27, 28], structures were solved by the heavy atom method and refined against F^2. Full matrix least-squares refinement was carried out using standard procedures [29]. All atoms were located in the difference Fourier map during refinement. Hydrogen atoms, unless otherwise noted, were refined with their isotropic displacement parameters (U$_{iso}$) equal to 1.5U$_{iso}$ of the atom to which they are attached. Specific refinement details are reported below and CIF data are provided for all structures in the electronic supplementary material (ESM). All structures were checked for missed higher symmetry and twinning with *PLATON* [30] and were further validated using *CheckCIF*.

X-ray powder diffraction data were collected at room temperature using an Inel CPS-120 X-ray powder diffractometer outfitted with an XRG3000 Cu X-ray tube. Microcrystalline c,c,t-$[Pt(NH_3)_2Cl_2(OH)_2]$ was packed into a 0.5 mm outer diameter capillary and mounted on a clay pellet. The sample was rotated perpendicular to the X-ray beam and irradiated with Cu Kα radiation (λ = 1.54056 Å). Diffracted radiation was collected from 2θ = 0 to 120°. Data processing and baseline correction were performed using *WinPLOTR* [31]. The powder pattern of c,c,t-$[Pt(NH_3)_2Cl_2(OH)_2]$ was simulated from the low temperature single crystal structure using *Mercury*. Because the single crystal data were collected at 100 K and the powder data were collected at 298 K, a scaling formula was used to align the simulated pattern with the experimental pattern. The scaling formula $2\theta = 0.992(2\theta_{raw}) - 0.4168$ was determined empirically by least-squares regression. The non-shifted simulation data are shown in Fig. S1 together with the non-baseline corrected experimental data.

Computational Details

Group theoretical vibrational analyses were carried out by standard methods [32]. DFT calculations were performed using *Gaussian03* [33] and the hybrid functional PBE0 [34]. The Pople-type 6-31++g(d,p) basis set was used for non-platinum atoms and the LANL2DZ effective core potential (ECP) for the platinum atom to account for relativistic effects [35]. Geometry optimization of c,c,t-$[Pt(NH_3)_2Cl_2(OH)_2]$ was performed using coordinates required by the C_{2v} site symmetry demanded by the crystal structure reported here. Separate calculations were performed in which C_{2v} symmetry either was or was not enforced. Analytical vibrational calculations were conducted to determine whether the optimized structures were truly minima on their respective potential energy surfaces. Raman intensities were computed by numerical differentiation of the analytic dipole derivatives with respect to an electric field.

Results and Discussion

Synthesis of Platinum Compounds

The pseudo-octahedral complex c,c,t-$[Pt(NH_3)_2Cl_2(OH)_2]$ was prepared by reaction of square-planar cis-$[Pt(NH_3)_2Cl_2]$ with hydrogen peroxide in water. Initially, a single H_2O_2 molecule attacks one face of the Pt(II) starting material, providing the first coordinated hydroxide ligand. The second hydroxide derives from a water molecule solvating the opposite face of the complex, trans to the attacking hydrogen peroxide [36]. The product of the reaction displays a great tendency to co-crystallize with hydrogen peroxide, particularly under common reaction conditions in which H_2O_2 is present in large excess. The large, well-formed crystals of the hydrogen peroxide solvate, or perhydrate, can be readily isolated, but the presence of H_2O_2 in the crystals can complicate subsequent reactivity. To obtain the unsolvated form, the solid material collected from the reaction mixture, ostensibly a mixture of c,c,t-$[Pt(NH_3)_2Cl_2(OH)_2]$ and c,c,t-$[Pt(NH_3)_2Cl_2(OH)_2]\cdot H_2O_2$, is stirred in boiling water. The thermal energy initiates degradation of the peroxide and permits partial dissolution of c,c,t-$[Pt(NH_3)_2Cl_2(OH)_2]$. Upon cooling to room temperature, clean samples of microcrystalline c,c,t-$[Pt(NH_3)_2Cl_2(OH)_2]$ are obtained, free of hydrogen peroxide. The composition and polymorphic purity of this material was assessed by comparing its powder diffraction pattern with that simulated from single crystal X-ray diffraction data (Fig. 1). The

lack of additional peaks in the experimental pattern, compared to that of the simulated one, confirms that the bulk crystalline material has the same three-dimensional structure as the one determined for a single crystal of the compound (*vide infra*).

Although a more detailed discussion of the vibrational spectroscopy of this compound will be presented below, we briefly highlight here the functional importance of this technique in monitoring the reactivity of this synthon. The IR spectrum of *c,c,t*-[Pt(NH$_3$)$_2$Cl$_2$(OH)$_2$] displays a sharp, intense O–H stretching band at 3516 cm^{-1}. The broad shoulder of variable intensity observed at 3450 cm^{-1} arises from adventitious water. The presence of hydrogen peroxide in the lattice of *c,c,t*-[Pt(NH$_3$)$_2$Cl$_2$(OH)$_2$]·H$_2$O$_2$ contributes two additional peaks, at 3470 and 3458 cm^{-1}, allowing facile detection of contamination by the perhydrate (Fig. 2). Moreover, this band provides a convenient handle by which to assess consumption of the molecule in subsequent chemistry. Typical reactions using *c,c,t*-[Pt(NH$_3$)$_2$Cl$_2$(OH)$_2$] as a synthetic intermediate involve nucleophilic attack of the hydroxide ligand on an electrophilic center, followed by scission of the O–H bond and disappearance of the O–H stretching band in the IR spectrum [2].

Crystallographic Analysis

Despite the ease with which the perhydrate forms large, well-facetted crystals, its structure [22] was reported only after that of the non-solvated complex appeared [18]. We supply here a redetermination of both structures together with the attendant crystallographic information files (see ESM). Certain features of the redetermined structures merit discussion.

The low temperature structure of *c,c,t*-[Pt(NH$_3$)$_2$Cl$_2$(OH)$_2$]·H$_2$O$_2$ presented here is consistent with that previously reported [22]. There is no significant difference in any of the heavy atom bond lengths or angles, although the quality of the new data permitted unrestrained refinement of the hydrogen atom positions. The refined N–H bond lengths are 0.877(6), 0.894(6), and 0.902(6) Å. The O–H distance in the hydrogen peroxide molecule is 0.786(6) Å and that in the platinum complex is 0.736(6) Å. In the previously reported structure, the hydrogen atoms of the ammine and the hydrogen peroxide were located in the difference Fourier synthesis, but that of the platinum-coordinated hydroxide was not. This hydrogen atom was explicitly located in the present structure and its position is consistent with that suggested by the two hydrogen bonding interactions of the hydroxide with an ammine ligand from a neighboring complex and a hydrogen peroxide of solvation. This positioning of the hydrogen atom does not permit any strong hydrogen bond donations, but a weak interaction is present with an O···Cl distance of 3.2448(17) Å and an O–H–Cl angle of 149(3)°. The final model refined to a residual index R$_1$ of 0.0098 for 1016 unique reflections obtained after merging for Fourier analysis (R$_1$ = 1.00% for the 1002 reflections having I > 4σ). Refinement details are presented in Table 1 and the structure is depicted in Fig. 3.

In the structures of *c,c,t*-[Pt(NH$_3$)$_2$Cl$_2$(OH)$_2$] first reported by Rosenberg and Lock [18] and subsequently at higher resolution by Sadler and coworkers [19], the space group was assigned as *P*4$_2$/*n*. The low temperature structure that we report here was, however, solved in *P*4$_2$/*nmc*. This choice was made on the basis of the systematically absent *hhl* reflections with *l* odd. These reflections are extinguished by the *c*-glide plane that is present in *P*4$_2$/*nmc* but not *P*4$_2$/*n*. Moreover, the observed Laue symmetry was clearly 4/*mmm* and not 4/*m*. This

change in space group was also suggested by Marsh [20]. The general features of our low temperature structure of *c,c,t*-[Pt(NH$_3$)$_2$Cl$_2$(OH)$_2$] are consistent with those of the two structures previously reported. The hydrogen atoms could be located in the difference Fourier maps, however, which was not possible in either of the previous two structures. The final hydrogen atom positions included in the model were obtained by semi-free refinement using a riding model. A more detailed discussion of these atomic positions is provided below in the context of their effect on the vibrational spectra of the complex. Refinement details are presented in Table 1 and the structure is depicted in Fig. 3.

Vibrational Analysis of c,c,t-[Pt(NH$_3$)$_2$Cl$_2$(OH)$_2$]

The original crystal structure reported for *c,c,t*-[Pt(NH$_3$)$_2$Cl$_2$(OH)$_2$] was used to interpret vibrational spectra, both IR and Raman, that had been acquired using the crystalline substance. One issue that the present structure addresses is the observed multiplicity of bands arising from N–H vibrations. Using possible hydrogen bonding patterns, Rosenberg and Lock deduced the potential positions for the hydrogen atoms, positions that remained undetermined in subsequent work by Sadler and coworkers. It was postulated that two of the ammine hydrogen atoms were directed towards oxygen atoms of hydroxyl groups of different neighboring molecules. The third ammine hydrogen would then be directed toward the chloride ligand of a neighboring molecule forming a hydrogen bonding interaction much weaker than those with the hydroxide ligands. The two distinct types of N–H hydrogen bonding interactions lift the degeneracy of the otherwise equivalent ammine hydrogen atoms and produce multiplicity in the N–H stretching, rocking, and wagging modes, as previously described [18]. The refined positions of the hydrogen atoms in the present structure confirm this interpretation. The ammine N–H group directed toward the chlorine atom lies on the mirror plane parallel to *ac*. The remaining two hydrogen atoms, which form hydrogen bonds to hydroxyl groups, are crystallographically related to each other by this mirror plane.

In the original treatment [18], the hydrogen atom on the hydroxide ligand was inferred to be disordered across a number of positions as judged by shoulders on the ν_{O-H} band observed at 3516 cm^{-1} in the IR and Raman spectra. The present crystal structure shows electron density arising from this hydrogen atom at a single position. Moreover, this position corresponds to that predicted based on the geometry of the hydrogen bonding interactions of the hydroxide with neighboring ammine ligands. The refined hydroxide hydrogen atom position completes a pseudo-tetrahedral geometry about the oxygen atom. This orientation of the hydroxide ligand places the hydrogen atom on a mirror plane and equally between two chloride ligands from different adjacent molecules. It is possible that the shoulders observed on the 3516 cm^{-1} band arise from slight coupling of the O–H oscillator to the strongly hydrogen bound N–H oscillators of adjacent molecules. The computational results presented below confirm that strong hydrogen bonding is occurring within the crystal, although a full factor group analysis was not carried out. Because the platinum atom sits on a special position, these are the only crystallographically independent hydrogen atoms.

Another aspect of the vibrational analysis about which we wish to expand is the assignment of the main skeletal vibrational modes, those involving Pt and atoms in the primary coordination sphere. In the original structure determination in *P*4$_2$/*n*, the site symmetry of

the platinum complex was C_2. This point group requires the presence of 6 skeletal vibrations of symmetry $3A + 3B$. Specifically, the Pt–N, Pt–Cl, and Pt–O vibrations are all $A + B$. These six vibrations are both Raman and IR allowed. In the original assignment, the Pt–Cl bands were easily identified because they occur at much lower energy than the Pt–N and Pt–O bands. If the NH_3 and OH groups are treated as point masses, then the near equivalence of the corresponding reduced masses of the Pt–NH_3 and Pt–OH harmonic oscillators prevents a straightforward assignment of the four signals in the 400–700 cm^{-1} range (Fig. 4). Rosenberg and coworkers proposed a tentative assignment based on the relative shifts in the energies of these transitions upon deuteration. The IR spectrum of the deuterated complex, however, is "missing" a band (Fig. 4). In the [1]H-containing sample, there is a shoulder at 575 cm^{-1}, a strong peak at 559 cm^{-1}, a medium intensity peak at 531 cm^{-1}, and a strong peak at 458 cm^{-1}. After deuterium exchange, the first three shift to 558, 534, and 497 cm^{-1}, respectively. There is, however, no peak corresponding to the shifted 458 cm^{-1} signal. The authors of the previous study used the magnitudes of the deuterium-induced shifts to assign the 559 cm^{-1} and 575 (shoulder) cm^{-1} bands to Pt–O vibrations and the 531 and 458 cm^{-1} bands to Pt–N vibrations. This degree of shift would predict that the 458 cm^{-1} signal would appear at approximately 428 cm^{-1}. No explanation is offered for the so-called "missing band" [18].

We were intrigued by the possibility that a reinterpretation of the vibrational spectroscopy in light of the corrected space group assignment could provide an explanation for the disappearance of the 458 cm^{-1} band upon deuteration. In space group $P4_2/nmc$, the platinum complex sits on a special position with site symmetry C_{2v}.

A group theoretical stretch mode analysis of the complex using point group C_{2v} reveals that, again, six skeletal stretching vibrations are expected. The vibrations, shown in Fig. 5, are of symmetry $A_1 + B_2$ (Pt–Cl), $A_1 + B_2$ (Pt–N), and $A_1 + B_1$ (Pt–O). All six vibrations are again predicted to be both IR and Raman active. Although no significant differences are apparent in this new analysis, inspection of the symmetry of the vibrational modes (*vide infra*) affords further corroboration of the assignment of the peaks in the 400–700 cm^{-1} range.

The two Pt–O vibrations correspond to the symmetric (A_1) and asymmetric (B_1) stretches (Fig. 5). Intuitively, one would expect the symmetric stretch to be IR inactive/Raman active and the asymmetric stretch to be IR active/Raman inactive. Such a conclusion follows from simple inspection of the changes in molecular dipole moment and molecular volume over the course of the vibration. The predicted combination of Raman and IR activity for both vibrations is therefore puzzling until it is realized that the linearity of the O–Pt–O fragment is not required by the C_{2v} point group; the crystallographically determined angle is, in fact, 177.16(15)°.

In order to account for the approximate O–Pt–O linearity not imposed by C_{2v} symmetry, the vibrations of fragments of the molecule were analyzed in isolation (Fig. 6). The N–Pt–N fragment has C_{2v} symmetry and a stretch mode analysis reveals vibrational modes of $A_1 + B_2$ symmetry that are both IR and Raman active. The same result obtains for the Cl–Pt–Cl fragment. The O–Pt–O fragment, however, has approximate $D_{\infty h}$ symmetry. Stretch mode analysis of this fragment reveals two vibrations of approximate A_{1g} (Σ^+_g) and A_{1u} (Σ^+_u)

symmetry. The former describes the symmetric stretch, A_1 in the parent molecule, and the latter the asymmetric stretch, B_1 in the parent molecule. The O–Pt–O fragment is approximately centrosymmetric and thus the IR/Raman mutual exclusion rule is approximately obeyed. The strong 559 cm^{-1} IR band coincides with a weak Raman signal and the 575 cm^{-1} shoulder coincides with a very intense Raman peak [18]. The 559 cm^{-1} band is therefore assigned as the A_1 Pt–O stretch and the 575 cm^{-1} shoulder as the B_1 symmetric mode.

This group theoretical analysis of the Pt–O vibrations can be further confirmed using modern computational chemistry. The structure of the molecule was optimized by DFT methods. If the geometry of the molecule is constrained to remain in point group C_{2v} during optimization, the converged structure is not a minimum on the potential energy surface. This feature was revealed by a frequency calculation, which identified two vibrations with imaginary frequencies. These two modes can be viewed as O–H wagging and twisting, although it is perhaps more illustrative to describe them as symmetric and asymmetric deformations about the Pt–O torsion angle (see ESM). This result suggests that the molecular geometry present in the crystal is not the most stable, but rather has the hydrogen atoms locked into higher energy positions by an extensive network of *inter*molecular hydrogen bonds. Because neither of these two vibrational modes involves a significant displacement of the skeletal oxygen atoms, the general symmetry information obtained about skeletal vibrations from a frequency calculation at this geometry is still valid. The geometry was, however, reoptimized without any constraints in order to obtain more rigorously correct vibrational data.

The calculations recovered the two Pt–O vibrations with symmetries A_1 and B_1. Although both are formally allowed, the A_1 vibration (symmetric stretch) is essentially IR inactive, and the B_1 vibration (asymmetric stretch) is essentially Raman inactive. For the former mode, the IR intensity is calculated to be 0.006% of the intensity of the strongest band and, for the latter mode, the Raman intensity is calculated to be 0.07% of that of the strongest band. The full computational output is provided in the ESM.

The computed spectral intensities also provide insight into the identities of the 531 and 458 cm^{-1} bands. The band arising from the symmetric Pt–N stretch is computed to be less intense than the asymmetric band in the IR and the converse is predicted for the Raman spectrum. These results, in conjunction with the reported IR and Raman spectra, are consistent with the assignment of the 531 cm^{-1} band as the A_1 vibration and the 458 cm^{-1} band as the B_2 vibration. The 458 cm^{-1} band is that which disappears upon deuterium exchange. Because the point masses of NH_3 and OH are very close to one another, it may have been possible to attribute the diminished intensity of the missing band to coupling to one of the Pt–O or Pt–N skeletal stretching modes that is pseudo forbidden, e.g. the A_1 Pt–O stretch. None of these stretching modes, however, has the appropriate B_2 symmetry.

Full vibrational analysis of the $PtO_2Cl_2N_2$ core with C_{2v} symmetry reveals that there are, however, lower energy deformation modes with B_2 symmetry. Specifically, the $3N-6 = 15$ skeletal vibrations are $6A_1+2A_2+3B_1+4B_2$. After removal of the stretching modes previously

determined, there remain nine vibrations of symmetry $3A_1 + 2A_2 + 2B_1 + 2B_2$, as shown in Fig. 7.

In the original vibrational analysis, these lower energy deformations can give rise to combination bands in 400–700 cm^{-1} region [18]. If a combination band of B_2 symmetry were to "accidentally" coincide in energy with the B_2 Pt–N band, then the Fermi resonance between them may result in significant attenuation of the Pt–N band. In order for the combination band to have the appropriate symmetry, the direct product of the irreducible representations of the two constituent bands must be B_2. In the C_{2v} point group, this product can be achieved with either $A_1 \times B_2$ or $A_2 \times B_1$. Although all nine of the non-stretching skeletal vibrations, with their appropriate symmetries, can be obtained from a DFT frequency calculation, not all can be identified in the experimental vibrational spectra [18]. It is therefore not possible to use the computational information to assign even those few bands that were identified. Among these low energy modes previously observed by IR and Raman, however, there are vibrations with the symmetry required to form a B_2 symmetric combination band. The 190 cm^{-1} mode, observed to form a combination band by Rosenberg and coworkers, is predicted to shift to approximately 180 cm^{-1} upon deuteration. It could combine with the 248 cm^{-1} band observed in the IR spectrum of the deuterated compound to give rise to a signal at 428 cm^{-1}. This position is exactly that predicted for the 450 cm^{-1} band if it shifts by the same factor as the 535 cm^{-1} Pt–N band upon deuteration.

Conclusions

The results presented facilitate reexamination of the vibrational analysis of *c,c,t-*[Pt(NH$_3$)$_2$Cl$_2$(OH)$_2$]. The vibrational spectroscopy of this molecule, an important synthon in the field of platinum anticancer chemistry, was first systematically explored by Rosenberg and coworkers [18]. An X-ray crystal structure determination allowed these authors to conduct a site group vibrational analysis of the molecule, which they used to partially assign IR and Raman spectra. The resolution of the previously determined structure prevented a detailed discussion of the influence of hydrogen bonding within the crystal on the fine structure of the N–H and O–H stretching bands. The presently reported high-resolution structure helps explain these features. The authors of the original analysis found that, following deuteration, one of the skeletal stretching bands disappeared. Reevaluation of the vibrational analysis with the correct site symmetry did not explicitly account for the "missing band" but did allow for a more definitive assignment of the nature and symmetry of every Pt–O and Pt–N stretching band. Following identification of the symmetry of the disappearing Pt–N band, we propose that shifts in peaks following deuteration allows for Fermi resonance with a combination band, resulting in significant attenuation of the intensity of the Pt–N mode.

Acknowledgments

References

1. Hall MD, Mellor HR, Callaghan R, Hambley TW. J Med Chem. 2007; 50:3403–3411. [PubMed: 17602547]

2. Giandomenico CM, Abrams MJ, Murrer BA, Vollano JF, Rheinheimer MI, Wyer SB, Bossard GE, Higgins JD III . Inorg Chem. 1995; 34:1015–1021. [PubMed: 20000850]

3. Barnes KR, Kutikov A, Lippard SJ. Chem Biol. 2004; 11:557–564. [PubMed: 15123250]

4. Reithofer M, Galanski M, Roller A, Keppler BK. Eur J Inorg Chem. 2006:2612–2617.

5. Olszewski U, Ach F, Ulsperger E, Baumgartner G, Zeillinger R, Bednarski P, Hamilton G. Met-Based Drugs. 2009; 2009:1–11.

6. Hall MD, Hambley TW. Coord Chem Rev. 2002; 232:49–67.

7. Battle AR, Choi R, Hibbs DE, Hambley TW. Inorg Chem. 2006; 45:6317–6322. [PubMed: 16878941]

8. Zhang JZ, Wexselblatt E, Hambley TW, Gibson D. Chem Commun. 2012; 48:847–849.

9. Singin AS, Mas'ko AS, Moldavanova LK, Lobanova EA, Serebryakov NG. Pharm Chem J. 1985; 19:589–593.

10. Carr JL, Tingle MD, McKeage MJ. Cancer Chemother Pharmacol. 2002; 50:9–15. [PubMed: 12111106]

11. Gray HB, Banci L, Luchinat C, Turano P. Nat Struct Mol Biol. 2012; 19:868–869.

12. Sabatini A, Bertini I. Inorg Chem. 1965; 4:959–961.

13. Sabatini A, Bertini I. Inorg Chem. 1966; 5:204–206.

14. Sabatini A, Bertini I. Inorg Chem. 1965; 4:1665–1667.

15. Bertini I, Sabatini A. Inorg Chem. 1966; 5:1025–1028.

16. Beattie IR. Chem Soc Rev. 1975; 4:107–153.

17. Dyer, RB.; Woodruff, WH. Encyclopedia of inorganic and bioinorganic chemistry. John Wiley & Sons, Ltd; 2011.

18. Faggiani R, Howard-Lock HE, Lock CJL, Lippert B, Rosenberg B. Can J Chem. 1982; 60:529–534.

19. Kuroda R, Neidle S, Ismail IM, Sadler PJ. Inorg Chem. 1983; 22:3620–3624.

20. Marsh RE. Inorg Chem. 1984; 23:2363–2363.

21. Tschugájeff L, Chlopin W, Fritzmann E. Z Anorg Allg Chem. 1926; 151:253–268.

22. Vollano JF, Blatter EE, Dabrowiak JC. J Am Chem Soc. 1984; 106:2732–2733.

23. APEX2, Apex2. Bruker AXS, Inc; Madison, WI: 2008.

24. SAINT, Saint: Sax area-detector integration program. University of Göttingen; Göttingen, Germany: 2008.

25. Sheldrick, GM. Sadabs: Area-detector absorption correction. University of Göttingen; Göttingen, Germany: 2008.

26. XPREP. Xprep. Bruker AXS; Madison, WI: 2008.

27. Sheldrick, GM. Shelxtl-97. University of Göttingen; Göttingen, Germany: 2000.

28. Sheldrick GM. Acta Crystallogr Sect A. 2008; 64:112–122. [PubMed: 18156677]

29. Müller P. Crystallogr Rev. 2009; 15:57–83.

30. Spek, AL. Platon, a multipurpose crystallographic tool. Utrecht University; Utrecht, The Netherlands: 2008.

31. Roisnel T, Rodriguez-Carvajal J. Mater Sci Forum. 2001; 378–381:118–123.

32. Cotton, FA. Chemical applications of group theory. Wiley; New York: 1990.

33. Frisch, MJ.; Trucks, GW.; Schlegel, HB.; Scuseria, GE.; Robb, MA.; Cheeseman, JR.; Montgomery, J.; JA; Vreven, T.; Kudin, KN.; Burant, JC.; Millam, JM.; Iyengar, SS.; Tomasi, J.; Barone, V.; Mennucci, B.; Cossi, M.; Scalmani, G.; Rega, N.; Petersson, GA.; Nakatsuji, H.; Hada, M.; Ehara, M.; Toyota, K.; Fukuda, R.; Hasegawa, J.; Ishida, M.; Nakajima, T.; Honda, Y.; Kitao, O.; Nakai, H.; Klene, M.; Li, X.; Knox, JE.; Hratchian, HP.; Cross, JB.; Adamo, C.; Jaramillo, J.; Gomperts, R.; Stratmann, RE.; Yazyev, O.; Austin, AJ.; Cammi, R.; Pomelli, C.;

Ochterski, JW.; Ayala, PY.; Morokuma, K.; Voth, GA.; Salvador, P.; Dannenberg, JJ.; Zakrzewski, VG.; Dapprich, S.; Daniels, AD.; Strain, MC.; Farkas, O.; Malick, DK.; Rabuck, AD.; Raghavachari, K.; Foresman, JB.; Ortiz, JV.; Cui, Q.; Baboul, AG.; Clifford, S.; Cioslowski, J.; Stefanov, BB.; Liu, G.; Liashenko, A.; Piskorz, P.; Komaromi, I.; Martin, RL.; Fox, DJ.; Keith, T.; Al-Laham, MA.; Peng, CY.; Nanayakkara, A.; Challacombe, M.; Gill, PMW.; Johnson, B.; Chen, W.; Wong, MW.; Gonzalez, C.; Pople, JA. Gaussian 03. Gaussian, Inc; Pittsburgh PA: 2003.

34. Adamo C, Barone V. J Chem Phys. 1999; 110:6158–6170.

35. Hay PJ, Wadt WR. J Chem Phys. 1985; 82:299–310.

36. Dunham SO, Larsen RD, Abbott EH. Inorg Chem. 1993; 32:2049–2055.
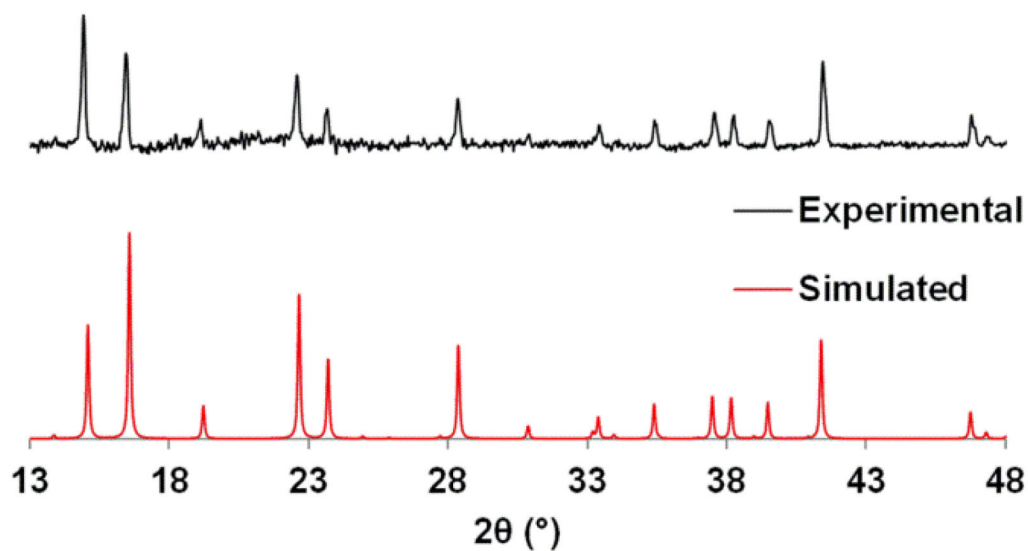
Fig. 1.
X-ray powder diffraction from a recrystallized sample of c,c,t-[Pt(NH$_3$)$_2$Cl$_2$(OH)$_2$] together
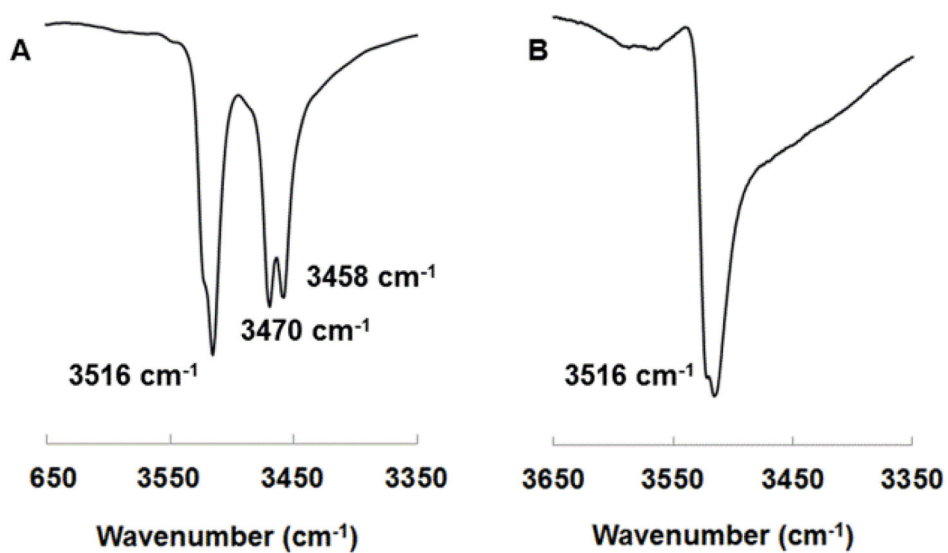with the simulated spectrum generated from the single crystal X-ray structure

Fig. 2.
IR spectra of c,c,t-[Pt(NH$_3$)$_2$Cl$_2$(OH)$_2$] with (**A**) and without (**B**) perhydrate contamination
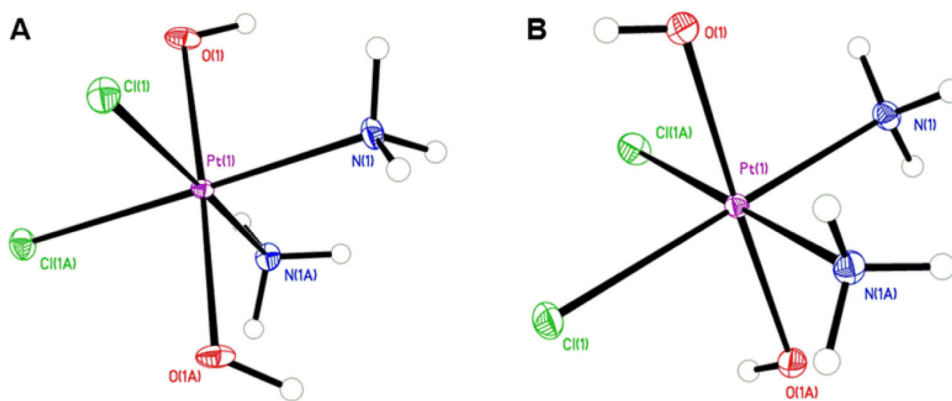
Fig. 3.
Molecular diagrams of the platinum complex from the crystal structures of (**A**) *c,c,t*-[Pt(NH$_3$)$_2$Cl$_2$(OH)$_2$] and (**B**) *c,c,t*-[Pt(NH$_3$)$_2$Cl$_2$(OH)$_2$]·H$_2$O$_2$ with thermal ellipsoids drawn at the 50% probability level
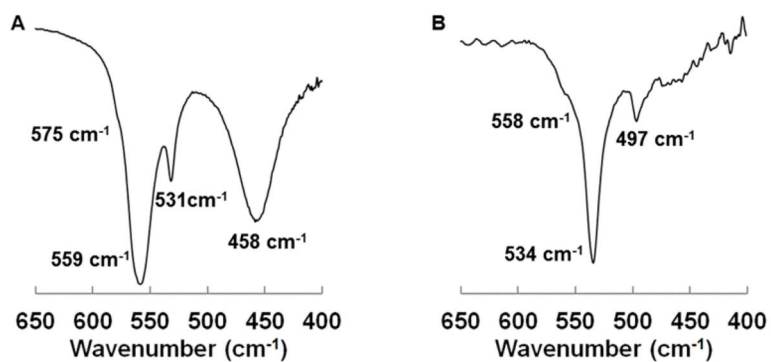
Fig. 4.
IR spectra of the 400–700 cm^{-1} region of (**A**) c,c,t-[Pt(NH$_3$)$_2$Cl$_2$(OH)$_2$] and (**B**) c,c,t-[Pt(ND$_3$)$_2$Cl$_2$(OD)$_2$]
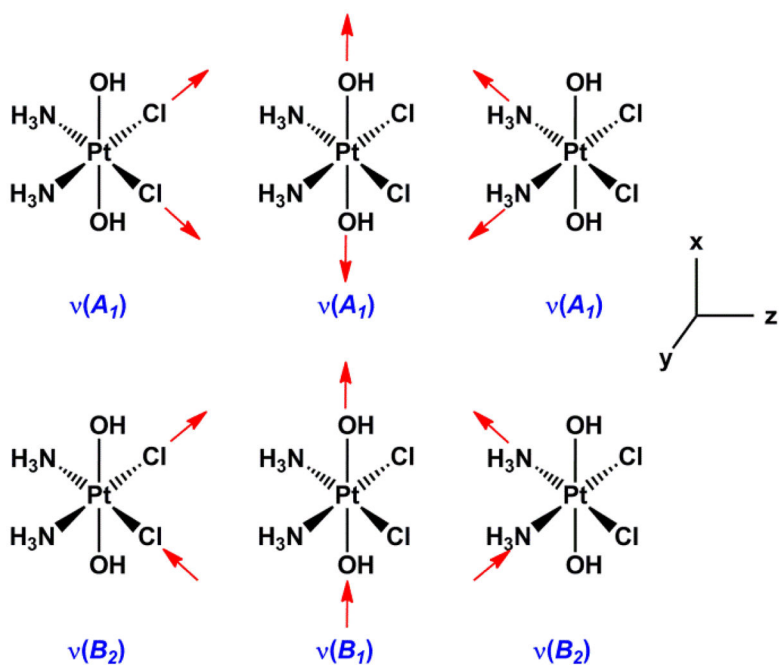
Fig. 5.
Normal coordinate skeletal stretching modes of c,c,t-[Pt(NH$_3$)$_2$Cl$_2$(OH)$_2$]
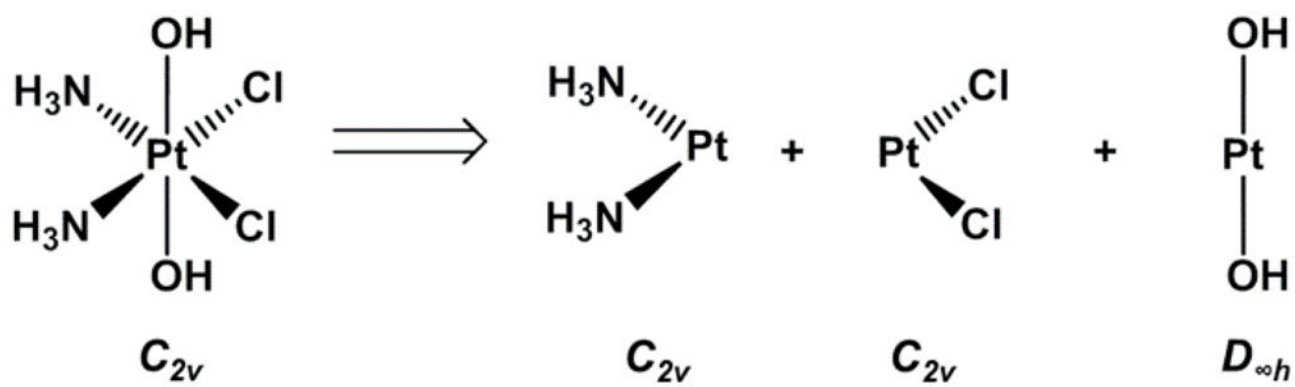
Fig. 6.
Hypothetical decomposition of c,c,t-[Pt(NH$_3$)$_2$Cl$_2$(OH)$_2$] into decoupled oscillators with their respective symmetries
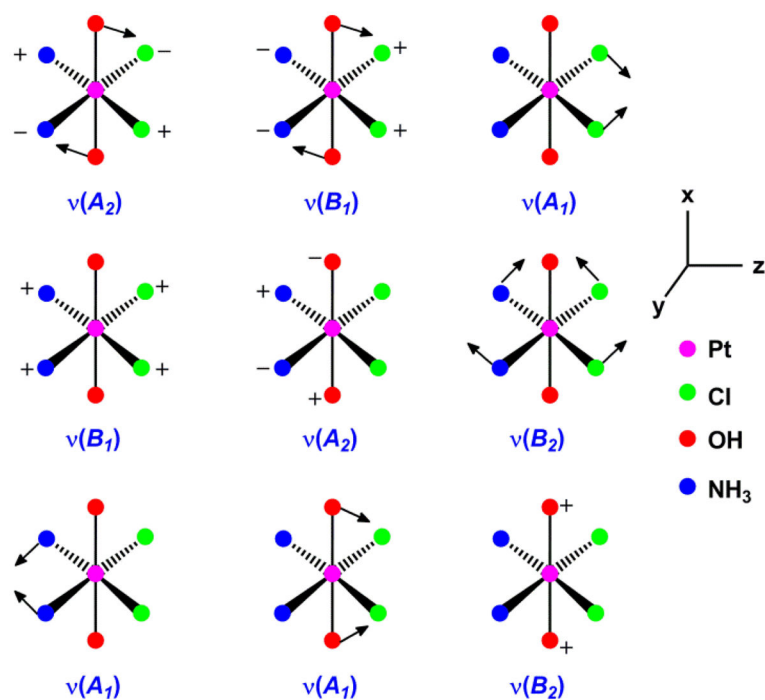
Fig. 7.
Normal coordinate non-stretching skeletal deformation modes of c,c,t-[Pt(NH$_3$)$_2$Cl$_2$(OH)$_2$]

Table 1

Crystallographic parameters for c,c,t-[Pt(NH$_3$)$_2$Cl$_2$(OH)$_2$] and c,c,t-[Pt(NH$_3$)$_2$Cl$_2$(OH)$_2$]·H$_2$O$_2$

	c,c,t-[Pt(NH$_3$)$_2$Cl$_2$(OH)$_2$]	c,c,t-[Pt(NH$_3$)$_2$Cl$_2$(OH)$_2$]·H$_2$O$_2$
Formula	Cl$_2$H$_8$N$_2$O$_2$Pt	Cl$_2$H$_8$N$_2$O$_2$Pt·H$_2$O$_2$
Formula weight	334.07	368.09
Space group	$P4_2/nmc$	$C2/c$
a, Å	7.3226(2)	11.1987(11)
b, Å	7.3226(2)	10.7472(11)
c, Å	11.3457(6)	7.1025(7)
β, °		115.2720(10)
V, Å^3	608.36(4)	773.01(13)
Z	4	4
T, K	100(2)	100(2)
μ(Mo Kα), mm^{-1}	23.844	18.800
θ range, °	3.31 to 28.71	2.76 to 28.84
total no. of data	11046	6832
no. of unique data	453	1016
no. of parameters	30	62
completeness to θ (%)	100	100
R$_1$[a] (%)	1.67	0.98
wR$_2$[b] (%)	5.01	2.24
GOF[c]	1.152	1.15
max, min peaks, e Å^{-3}	1.64 and −1.79	0.649 and −0.940

[a]R$_1$=Σ||F$_O$| - |F$_C$||/Σ|F$_O$|.

[b]wR$_2$={Σ [w(F$_O^2$-F$_C^2$)^2]/Σ [w(F$_O^2$)^2]}$^{1/2}$.

[c]GOF= {Σ [w(F$_O^2$-F$_C^2$)^2]/(n-p)}$^{1/2}$